frontiers

On the nature of the core of α Centauri A: the impact of the metallicity mixture

Benard Nsamba [1,2,*], **Tiago L. Campante** [1,2], **Mário J. P. F. G. Monteiro** [1,2], **Margarida S. Cunha** [1,2] **and Sérgio G. Sousa** [1,2]

[1] *Instituto de Astrofísica e Ciências do Espaço, Universidade do Porto, Rua das Estrelas, PT4150-762 Porto, Portugal*
[2] *Departamento de Física e Astronomia, Faculdade de Ciências da Universidade do Porto, PT4169-007 Porto, Portugal*

Correspondence*:
Benard Nsamba
benard.nsamba@astro.up.pt

arXiv:1904.01560v1 [astro-ph.SR] 2 Apr 2019

ABSTRACT

Forward asteroseismic modelling plays an important role towards a complete understanding of the physics taking place in deep stellar interiors. With a dynamical mass in the range over which models develop convective cores while in the main sequence, the solar-like oscillator α Centauri A presents itself as an interesting case study. We address the impact of varying the metallicity mixture on the determination of the energy transport process at work in the core of α Centauri A. We find that $\gtrsim 70\%$ of models reproducing the revised dynamical mass of α Centauri A have convective cores, regardless of the metallicity mixture adopted. This is consistent with the findings of Nsamba et al., where nuclear reaction rates were varied instead. Given these results, we propose that α Centauri A be adopted in the calibration of stellar model parameters when modelling solar-like stars with convective cores.

Keywords: HD 128620, Asteroseismology, Stellar modelling, Fundamental parameters, Convection, Radiation

1 INTRODUCTION

Most parameters used in stellar modelling are calibrated based on the Sun, e.g., the mixing length parameter, the helium-to-heavy-element ratio, chemical abundances etc. This approach is well-suited to the modelling of stars with similar properties to the Sun, i.e., for solar-type stars with a mass below 1.1 $M_\odot$. The quest for a more massive star with well-known properties and interior structure is of the utmost importance, as such star could become a potential model calibrator for solar-like stars having convection as the main energy transport process in their cores.

The bright, nearby binary α Centauri is amongst the best characterized star systems, with a plethora of available high-precision observations, e.g., parallaxes, angular diameters, interferometric radii, metallicities, effective temperatures, luminosities, and oscillation frequencies (Söderhjelm 1999; Pourbaix et al. 2002; Bouchy and Carrier 2002; Bedding et al. 2005; Bazot et al. 2007; de Meulenaer et al. 2010; Pourbaix and Boffin 2016; Kervella et al. 2016, 2017). α Centauri A is of particular interest, since its dynamical mass is in the range (1.1 – 1.15 $M_\odot$; Aerts et al. 2010) over which models constructed at solar metallicity are expected to develop convective cores while in the main sequence. This has given rise

to studies that aimed at establishing the nature of its core and at exploring the physics that affect core properties.

Forward stellar modelling, when coupled with observational constraints from asteroseismology, constitutes a valuable tool in the exploration of the physics of stellar interiors (e.g., Miglio and Montalbán 2005; Mathur et al. 2012; Metcalfe et al. 2012, 2014; Lebreton and Goupil 2014; Silva Aguirre et al. 2015; Nsamba et al. 2018b). Bazot et al. (2016) complemented asteroseismic and spectroscopic observables with the dynamical mass determined by Pourbaix et al. (2002) to tightly constrain stellar models of α Centauri A. They explored the impact of varying the nuclear reaction rates, overshoot, and diffusion of hydrogen and helium, having found a noticeable change in the number of best-fit models[1] with convective cores when nuclear reaction rates were varied. Following the revision of the dynamical mass of α Centauri A (Pourbaix and Boffin 2016), Nsamba et al. (2018a) (hereafter Paper I) carried out a detailed modelling of this star again allowing the nuclear reaction rates to vary, and found about 70% of best-fit models to have convective cores. More recently, Joyce and Chaboyer (2018) suggested that, if α Centauri A has a convective core, then it would be necessary to modify standard physical prescriptions (e.g., enhancing diffusion) in order to correctly model the star. Amongst the different model physics explored in Paper I and in Bazot et al. (2016), the impact of the metallicity mixture on the core properties of α Centauri A has, however, not been investigated.

In this work we investigate the impact of the metallicity mixture on the inferred nature of the core of α Centauri A. The paper is organized as follows: Section 2 describes the stellar model grids and sets of observables used in the optimization process. A discussion of the results is presented in Sect. 3. Section 4 presents the conclusions.

2 MODEL GRIDS AND OBSERVATIONAL CONSTRAINTS

To explore the impact of varying the metallicity mixture on the nature of the core of α Centauri A, we set up two grids (A and B) with the same model physics except for the metallicity mixture (see Table 1). The stellar evolution code MESA (Modules for Experiments in Stellar Astrophysics; Paxton et al. 2011, 2013, 2015, 2018) version 9793 was used to generate the grids.

We set the metallicity mixture in Grid A according to Grevesse et al. (1998) with a solar surface heavy element mass fraction $Z_{\rm surface,\odot} = 0.016$, while Grid B uses the metallicity mixture from Asplund et al. (2009) with $Z_{\rm surface,\odot} = 0.0134$. The main motivation for considering these two mixtures goes back to the theoretically predicted sound speed profiles for solar models constructed with the different composition mixtures. Delahaye and Pinsonneault (2006) reported that solar models using the Grevesse et al. (1998) and Asplund et al. (2009) mixtures yield a sound speed profile close to that of the real Sun, as opposed to models that use the Asplund et al. (2005) mixture. We recall that the metallicity, [Fe/H], is defined as:

$$[\mathrm{Fe/H}] = \log\left(\frac{Z_{\rm surface}}{X_{\rm surface}}\right)_{\rm star} - \log\left(\frac{Z_{\rm surface}}{X_{\rm surface}}\right)_{\odot}, \quad (1)$$

where $X_{\rm surface}$ is the surface hydrogen mass fraction. Notice that varying the metallicity mixture requires setting the corresponding appropriate opacities. We used opacities from OPAL tables (Iglesias and Rogers 1996) at high temperatures, whereas at low temperatures tables from Ferguson et al. (2005) were used instead, for the respective metallicity mixtures. We employed the Joint Institute for Nuclear Astrophysics

[1] In this work, models that are representative of a set of observables are termed as best-fit models.

Reaction Library (JINA REACLIB; Cyburt et al. 2010) in both grids. The $^{14}\mathrm{N}(p,\gamma)^{15}\mathrm{O}$ and $^{12}\mathrm{C}(\alpha,\gamma)^{16}\mathrm{O}$ rates were described according to Imbriani et al. (2005) and Kunz et al. (2002), respectively. We note that the $^{12}\mathrm{C}(\alpha,\gamma)^{16}\mathrm{O}$ reaction rate is less relevant for stars on the main-sequence phase but is vital in more evolved stars, i.e., stars at the core helium-burning evolution stage. Table 1 lists the macrophysics

Table 1. Main features of the model grids adopted in this work.

Grid	Metallicity Mixture	Core Overshoot	Diffusion
A	Grevesse et al. (1998)	Yes	Yes
B	Asplund et al. (2009)	Yes	Yes

used in either grid. We note that core overshoot was included as described by Herwig (2000) for models identified to have developed convective cores. Atomic diffusion was included in all our models according to Thoul et al. (1994). The latter is known to be a vital chemical transport process in low-mass stars (e.g., Silva Aguirre et al. 2017; Nsamba et al. 2018b). The mixing length theory, as described by Böhm-Vitense (1958), was used to describe convection. We also implemented the Grey–Eddington atmosphere to integrate the atmospheric structure from the photosphere to an optical depth of 10^{-4}. The helium mass fraction (Y) was estimated using the relation

$$Y = Z\left(\frac{\Delta Y}{\Delta Z}\right) + Y_0\,, \tag{2}$$

where $\Delta Y/\Delta Z$ is the helium-to-heavy-element relation (set to 2.0; Serenelli and Basu 2010) and Y_0 is the big bang nucleosynthesis value (set to 0.2484; Cyburt et al. 2003).

Evolutionary tracks were evolved from the zero-age main sequence to the end of the subgiant evolution phase. The terminal criterion affecting the tracks is similar to that implemented in Paper I. The parameter space of the model grids is as follows: $M \in [1.0, 1.2]$ $\mathrm{M}_\odot$ in steps of 0.01 $\mathrm{M}_\odot$; mixing length parameter, $\alpha_{\mathrm{mlt}} \in [1.3, 2.5]$ in steps of 0.1; overshoot parameter, $f_{\mathrm{ov}} \in [0, 0.03]$ in steps of 0.005; and $Z \in [0.023, 0.039]$ in steps of 0.005. Each model grid contains about 156,000 models. The corresponding adiabatic oscillation frequencies of each model, for spherical degrees l = 0, 1, 2, and 3, were determined using GYRE (Townsend and Teitler, 2013). The surface effects were accounted for using the combined-term surface correction method described by Ball and Gizon (2014). This surface correction method has been reported to yield the least internal systematic uncertainties among the different available corrections (e.g., Nsamba et al. 2018b; Compton et al. 2018; Jørgensen et al. 2019).

Table 2 displays the spectroscopic and interferometric constraints used in the optimization process. Run I adopts T_{eff} and [Fe/H] values obtained in Paper I. These spectroscopic constraints were complemented

Table 2. Spectroscopic and interferometric constraints.

Run	T_{eff} (K)	[Fe/H] (dex)	Radius ($\mathrm{R}_\odot$)
I	5832 ± 62	0.23 ± 0.05	1.2310 ± 0.0036
II	5795 ± 19	0.23 ± 0.05	1.2234 ± 0.0053

with the interferometric radius from Pourbaix and Boffin (2016). Run II adopts T_{eff} and interferometric radius values from Kervella et al. (2016). We further note that Pourbaix et al. (2002) derived a dynamical mass of 1.105 ± 0.0070 $\mathrm{M}_\odot$. This dynamical mass was then revised by Pourbaix and Boffin (2016), who obtained a value of 1.133 ± 0.0050 $\mathrm{M}_\odot$.

Finally, the same asteroseismic constraints as in Paper I were adopted. The Bayesian code AIMS (Asteroseismic Inference on a Massive Scale; Lund and Reese 2018; Rendle et al. 2019), a software for fitting stellar pulsation data, was used as our optimization tool. Stellar parameters and their associated uncertainties were taken as the mean and standard deviation of the resulting posterior probability distribution functions (PDFs), as output by AIMS.

3 DISCUSSION

Table 3 presents the stellar parameters determined using the model grids described in Table 1 and the sets of observables in Table 2. Our results show that we are able to reproduce the dynamical masses of Pourbaix and Boffin (2016) (Run I) and Pourbaix et al. (2002) (Run II) within 1σ (see Fig. 1 and Table 3). We note that the observed luminosity (i.e., 1.521 ± 0.015 $L_{\odot}$; Kervella et al. 2017) of α Centauri A was not included among the sets of observables as shown in Table 2. This is constrained via the combination of the interferometric radius and effective temperature. Our derived luminosity values are in agreement with the observed values (see Table 4). Run II and Run I luminosity values from both grids are consistent within 1σ and 2σ, respectively. The slight increase in luminosity values obtained in Run I is attributed to the larger interferometric radius used (see Table 2).

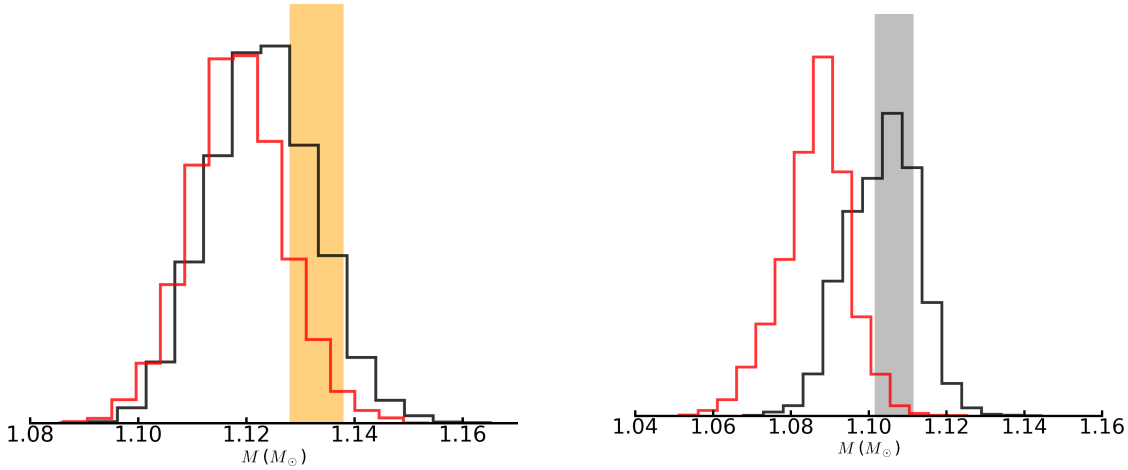


Figure 1. Run I (left) and Run II (right): Histograms represent the stellar mass posterior PDFs obtained using Grids A (red) and B (black). The dynamical masses (and corresponding uncertainties) of Pourbaix and Boffin (2016) and Pourbaix et al. (2002) are shown in orange and grey, respectively.

Table 3. Stellar parameters determined using different grids and observational constraints. The sixth column shows the percentage of best-fit models with convective cores, while the seventh column shows the upper convective-core mass limit.

Grid	Run	M ($M_{\odot}$)	t (Gyr)	$\alpha_{\rm mlt}$	Convective Core (%)	$M_{\rm c}$ ($M_{\odot}$)
A	I	1.12 ± 0.01	4.30 ± 0.35	1.97 ± 0.10	70	$\leqslant 0.085$
	II	1.09 ± 0.01	4.74 ± 0.40	1.76 ± 0.07	46	$\leqslant 0.084$
B	I	1.12 ± 0.01	4.72 ± 0.37	1.89 ± 0.10	79	$\leqslant 0.096$
	II	1.10 ± 0.01	4.73 ± 0.39	1.67 ± 0.07	79	$\leqslant 0.092$

A clear difference can be seen in the right panel of Fig. 1 (Run II) between the stellar mass posterior PDFs obtained using the two grids. Since varying the metallicity mixture has been shown to have a

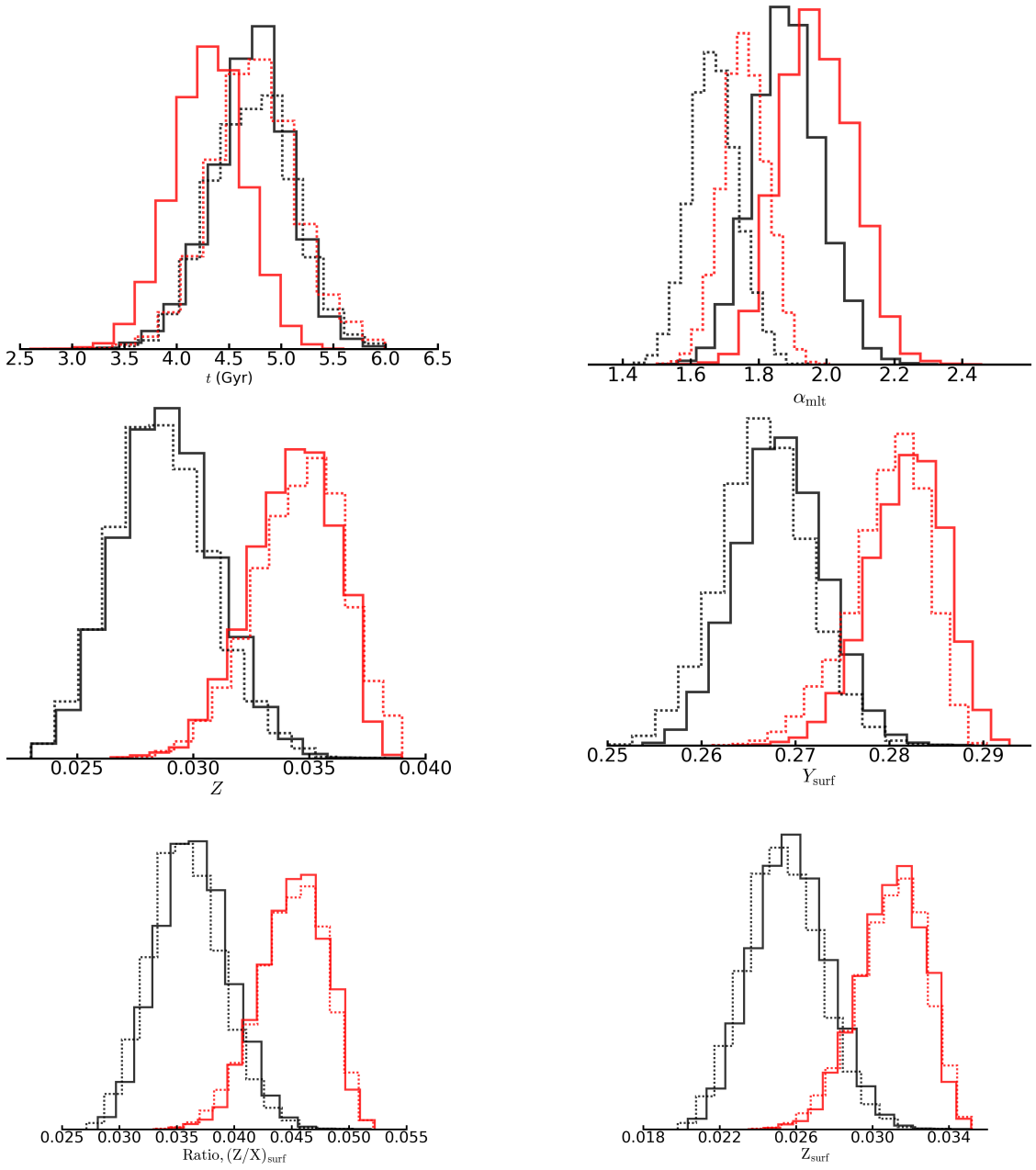


Figure 2. Histograms represent stellar parameter posterior PDFs obtained using different grids (Grid A in red and Grid B in black) and observational constraints (Run I as solid lines and Run II as dashed lines).

Table 4. Luminosities and abundances determined using different grids and observational constraints.

Grid	Run	L ($L_\odot$)	Z	$Y_{\rm surf}$	$Z_{\rm surf}$	$(Z/X)_{\rm surf}$
A	I	1.703 ± 0.059	0.034 ± 0.002	0.282 ± 0.004	0.031 ± 0.002	0.045 ± 0.003
	II	1.502 ± 0.023	0.035 ± 0.002	0.279 ± 0.004	0.031 ± 0.002	0.045 ± 0.003
B	I	1.675 ± 0.063	0.028 ± 0.002	0.269 ± 0.005	0.026 ± 0.002	0.036 ± 0.003
	II	1.510 ± 0.022	0.028 ± 0.002	0.267 ± 0.005	0.025 ± 0.002	0.036 ± 0.003

minimum effect on the estimated stellar mass (Silva Aguirre et al. 2015; Nsamba et al. 2018b), this feature can instead be explained by the different core properties of the best-fit models. Table 3 shows that the number of best-fit models with convective cores changes from 46% to 79% when the metallicity mixture is changed from that of Grevesse et al. (1998) to that of Asplund et al. (2009). This happens

since the dynamical mass of Pourbaix et al. (2002) lies within a range in which the onset of the CNO (carbon–nitrogen–oxygen) cycle, and thus core convection, is highly sensitive to the adopted metallicity mixture.

A different scenario is found when considering models that reproduce the dynamical mass of Pourbaix and Boffin (2016), with the stellar mass posterior PDFs showing excellent agreement (Run I; see left panel of Fig. 1). The percentage of models with convective cores is now consistent (i.e., $\gtrsim 70\%$) irrespective of the model grid adopted. We note that best-fit models are on average higher in mass compared to Run II and most have already developed convective cores, with any variation in the metallicity mixture generating no significant difference on their core properties.

In Table 3, we show the upper limits of the convective-core mass ($M_{\rm c}$) of our best-fit models. From all runs, we find the core radius to have an upper limit of 0.11 $\rm R_{\odot}$. Bazot et al. (2012) derived an upper limit for the radius and the mass of a possible convective core in α Centauri A to be 0.059 $\rm R_{\odot}$ and 0.035 $\rm M_{\odot}$, respectively. These limits were derived while taking into account the small frequency separation ($\delta\nu$) in the optimisation, as this parameter can provide a direct estimation of the convective core characteristics. Furthermore, when exploring the contribution of the different model physics to the nature of the core of α Centauri A, Bazot et al. (2016), in their table 3, report the core radius of their best-fit models to vary between 0.026 and 0.084 $\rm R_{\odot}$, which is consistent with our findings.

The top left panel of Fig. 2 shows that the derived stellar ages are in excellent agreement irrespective of the grid and observational constraints used. Furthermore, these ages are consistent with literature values (Kim 1999; Yıldız 2007; Bazot et al. 2016; Nsamba et al. 2018a; Joyce and Chaboyer 2018). Table 3 and the top right panel of Fig. 2 show that the $\alpha_{\rm mlt}$ estimated based on either Run I (solid lines) or Run II (dashed lines) are consistent within 1σ. The values of $\alpha_{\rm mlt}$ across runs are however different, this being mainly due to the different radius constraints used (see Table 2). We note that the interferometric radius measurements used in each run indirectly constrain the model mass. Moreover, $\alpha_{\rm mlt}$ is known to have a significant degree of correlation with the stellar mass and effective temperature (Pinheiro and Fernandes, 2013).

A clear contrast can be seen in the bottom panels of Fig. 2 between the best-fit models obtained using the two grids. As expected, the grid based on the metallicity mixture from Asplund et al. (2009) (Grid B) leads to best-fit models with a lower Z compared to those based on the mixture from Grevesse et al. (1998) (Grid A). A similar feature can be seen for the surface helium mass fraction, $Y_{\rm surf}$.

The model properties that influence the onset of the CNO cycle (and associated convective core) include the adopted physics, metallicity, and mass. As mentioned in Sect. 2, both grids contain the same physics apart from the metallicity mixture. We note that models with high metallicity have a higher chance of developing convective cores. This is because a high metallicity leads to an increase in opacity, which in turn reduces the efficiency of radiative energy transport. This ultimately results in an increase in core temperature which favours the onset of the CNO cycle. Similarly, models with a higher mass have higher core temperatures, hence higher chances of developing a convective core. The top left panel of Fig. 3 shows that best-fit models with high mass develop large and massive convective cores. This could be explained by their high overshoot parameter values as shown in the bottom panel of Fig 3. Best-fit models with $f_{\rm ov} = 0$ have smaller core masses and radii. The top right panel of Fig. 3 shows no clear trend regarding the contribution from the initial metal mass fraction. We note that consistent results as those in Fig. 3 are obtained when different runs are used.

It is interesting to assess the dominant model property that facilitates the occurrence of convective cores for the best-fit models in either run. Despite the high metallicity of best-fit models from Grid A (Run II) (see bottom left panel of Fig. 2), the majority of these models have masses $\lesssim 1.1$ M$_\odot$ (see right panel of Fig. 1) resulting into 46% of models with convective cores. Grid B (Run II) contains most of the best-fit models with low metallicity but with masses $\gtrsim 1.1$ M$_\odot$ (see right panel of Fig. 1), leading to 79% of models with convective cores. Hence, for Run II (both grids), model mass is the dominant model property responsible for the onset of the CNO cycle.

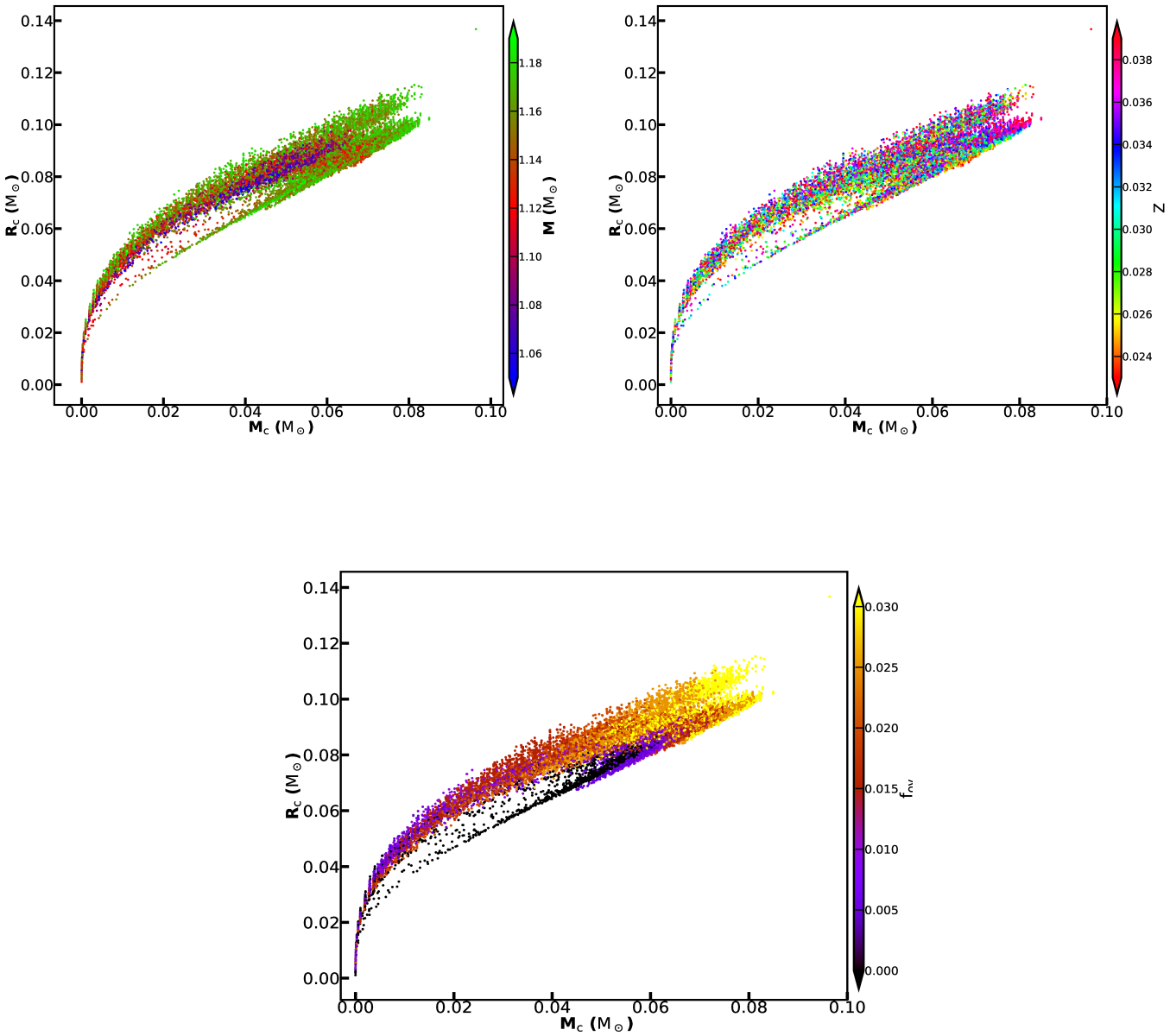


Figure 3. Scatter plots showing core radius (R_c) vs. core mass (M_c) for best-fit models with convective cores obtained using grid B (Run I). The top left panel is colour-coded according to the model mass (M), the top right panel according to the initial metal mass fraction (Z), and the bottom panel according to the overshoot parameter (f_{ov}).

For Grid A (Run I), it is challenging to determine the dominant model property that yields convective cores. This is because most of the best-fit models have masses $\gtrsim$ 1.1 $M_{\odot}$ and high metallicity (see left panel of Fig. 1 and bottom left panel of Fig. 2). However, for Grid B (Run I), the majority of best-fit models have low metallicity but masses $\gtrsim$ 1.1 $M_{\odot}$, with 79% of models having convective cores. Therefore, also in this case model mass is the dominant model property contributing to the onset of the CNO cycle. Further, our results show that the mass range over which models constructed at different metallicities are expected to develop convective cores is 1.05 – 1.15 $M_{\odot}$.

4 CONCLUSIONS

In Paper I we assessed the impact on the nature of the core of α Centauri A of varying the nuclear reaction rates, which showed that $\gtrsim$ 70% of best-fit models reproducing the revised dynamical mass of Pourbaix and Boffin (2016) have convective cores. In this article, we expanded on the previous work by exploring the impact of varying the metallicity mixture (and corresponding opacities). Our findings show that $\gtrsim$ 70% of best-fit models reproducing the revised dynamical mass have convective cores.

In sum, the percentage of best-fit models with convective cores remains above 70% when imposing the most up-to-date set of observational constraints. This happens irrespective of the adopted metallicity mixture and nuclear reaction rates. Therefore, we propose that α Centauri A be adopted in the calibration of stellar model parameters when modelling solar-like stars with small convective cores.

During the "standard" solar calibration process, the initial metal mass fraction (Z), initial helium mass fraction (Y), and the mixing length parameter ($\alpha_{\rm mlt}$) are varied until a model is attained that satisfies the observed oscillation frequencies, effective temperature, metallicity, luminosity, and radius at the current solar age. The same model physics and solar calibrated parameters are then used to create grids for modelling other stars. Unlike the case of the Sun, there is no model-independent age for α Centauri A, but we do have a precise dynamical mass, interferometric radius, effective temperature, metallicity, and luminosity. In addition, we currently have ground-based seismic data, with the quality of those data expected to improve following the star's planned observations by space-based missions such as NASA's Transiting Exoplanet Survey Satellite (TESS; Ricker et al. 2015; Campante et al. 2016) and ESA's PLAnetary Transits and Oscillations of stars (PLATO; Rauer et al. 2014). This will improve the precision of observed oscillation frequencies and is also expected to increase the number of oscillation frequencies for all observable spherical degrees (l). This will support a more comprehensive asteroseismic analysis than the one presented here and in Paper I.

Therefore, with all these sets of observables, it will be possible to carry out a calibration procedure similar to the "standard" solar calibration routine briefly described above, without having the age among the constraints. It will also be feasible to provide effective constraints on some aspects of the physics, namely convection (mixing length, overshoot, surface effects), diffusion and opacities. The potential for constraining reaction rates is also a possibility when two or all stellar components of this triple system have seismic data of high precision available.

FUNDING

This work was supported by FCT - Fundação para a Ciência e a Tecnologia through national funds and by FEDER through COMPETE2020 - Programa Operacional Competitividade e Internacionalização by these grants: UID/FIS/04434/2013 & POCI-01-0145-FEDER-007672, PTDC/FIS-AST/30389/2017 & POCI-01-0145-FEDER-030389 and PTDC/FIS-AST/28953/2017 & POCI-01-0145-FEDER-028953.

B. Nsamba is supported by Fundação para a Ciência e a Tecnologia (FCT, Portugal) under grant PD/BD/113744/2015 from PhD::SPACE, an FCT PhD program. T. L. Campante acknowledges support from the European Union's Horizon 2020 research and innovation programme under the Marie Skłodowska-Curie grant agreement No. 792848 (PULSATION) and from grant CIAAUP-12/2018-BPD. SGS acknowledges support from FCT through Investigador FCT contract No. IF/00028/2014/CP1215/CT0002 and from FEDER through COMPETE2020 (grants UID/FIS/04434/2013 & PTDC/FIS-AST/7073/2014 & POCI-01-0145 FEDER-016880). Based on data obtained from the ESO Science Archive Facility under request number SAF Alpha Cen A 86436. T

ACKNOWLEDGEMENTS

We acknowledge the referees for the helpful and constructive remarks. B. Nsamba would like to thank the MESA community for advice on how to handle specific issues regarding the fine-tuning of the MESA code so as to produce sensible results. B. Nsamba would also like to thank the members of the asteroseismology group at the Instituto de Astrofísica e Ciências do Espaço for their feedback, which added value to this work.

REFERENCES

Aerts, C., Christensen-Dalsgaard, J., and Kurtz, D. (2010). *Asteroseismology*. Astronomy and Astrophysics Library (Springer Netherlands)

Asplund, M., Grevesse, N., and Sauval, A. J. (2005). The Solar Chemical Composition. In *Cosmic Abundances as Records of Stellar Evolution and Nucleosynthesis*, eds. T. G. Barnes, III and F. N. Bash. vol. 336 of *Astronomical Society of the Pacific Conference Series*, 25

Asplund, M., Grevesse, N., Sauval, A. J., and Scott, P. (2009). The Chemical Composition of the Sun. *Annual Review of Astron and Astrophys* 47, 481–522. doi:10.1146/annurev.astro.46.060407.145222

Ball, W. H. and Gizon, L. (2014). A new correction of stellar oscillation frequencies for near-surface effects. *A&A* 568, A123. doi:10.1051/0004-6361/201424325

Bazot, M., Bouchy, F., et al. (2007). Asteroseismology of α Centauri A. Evidence of rotational splitting. *A&A* 470, 295–302. doi:10.1051/0004-6361:20065694

Bazot, M., Bourguignon, S., and Christensen-Dalsgaard, J. (2012). A Bayesian approach to the modelling of α Cen A. *MNRAS* 427, 1847–1866. doi:10.1111/j.1365-2966.2012.21818.x

Bazot, M., Christensen-Dalsgaard, J., Gizon, L., and Benomar, O. (2016). On the uncertain nature of the core of α Cen A. *MNRAS* 460, 1254–1269. doi:10.1093/mnras/stw921

Bedding, T. R., Kjeldsen, H., Bouchy, F., Bruntt, H., Butler, R. P., Buzasi, D. L., et al. (2005). The non-detection of oscillations in Procyon by MOST: Is it really a surprise? *A&A* 432, L43–L48. doi:10.1051/0004-6361:200500019

Böhm-Vitense, E. (1958). Über die Wasserstoffkonvektionszone in Sternen verschiedener Effektivtemperaturen und Leuchtkräfte. Mit 5 Textabbildungen. *Zeit. Astrophys.* 46, 108

Bouchy, F. and Carrier, F. (2002). The acoustic spectrum of alpha Cen A. *A&A* 390, 205–212. doi:10.1051/0004-6361:20020706

Campante, T. L., Schofield, M., Kuszlewicz, J. S., Bouma, L., Chaplin, W. J., Huber, D., et al. (2016). The Asteroseismic Potential of TESS: Exoplanet-host Stars. *ApJ* 830, 138. doi:10.3847/0004-637X/830/2/138

Compton, D. L., Bedding, T. R., Ball, W. H., Stello, D., Huber, D., White, T. R., et al. (2018). Surface correction of main-sequence solar-like oscillators with the Kepler LEGACY sample. *MNRAS* 479, 4416–4431. doi:10.1093/mnras/sty1632

Cyburt, R. H. et al. (2003). Primordial nucleosynthesis in light of WMAP. *Physics Letters B* 567, 227–234. doi:10.1016/j.physletb.2003.06.026

Cyburt, R. H. et al. (2010). The jina reaclib database: Its recent updates and impact on type-i x-ray bursts. *ApJS* 189, 240

de Meulenaer, P. et al. (2010). Core properties of α Centauri A using asteroseismology. *A&A* 523, A54. doi:10.1051/0004-6361/201014966

Delahaye, F. and Pinsonneault, M. H. (2006). The Solar Heavy-Element Abundances. I. Constraints from Stellar Interiors. *ApJ* 649, 529–540. doi:10.1086/505260

Ferguson, J. W., Alexander, D. R., et al. (2005). Low-Temperature Opacities. *ApJ* 623, 585–596. doi:10.1086/428642

Grevesse, N. et al. (1998). Standard Solar Composition. *Space Science Reviews* 85, 161–174. doi:10.1023/A:1005161325181

Herwig, F. (2000). The evolution of AGB stars with convective overshoot. *A&A* 360, 952–968

Iglesias, C. A. and Rogers, F. J. (1996). Updated Opal Opacities. *ApJ* 464, 943. doi:10.1086/177381

Imbriani, G., Costantini, H., et al. (2005). S-factor of ^{14}N(p,γ)^{15}O at astrophysical energies*. *EPJ A* 25, 455–466. doi:10.1140/epja/i2005-10138-7

Jørgensen, A. C. S., Weiss, A., Angelou, G., and Silva Aguirre, V. (2019). Mending the structural surface effect of 1D stellar structure models with non-solar metallicities based on interpolated 3D envelopes. *MNRAS* 484, 5551–5567. doi:10.1093/mnras/stz337

Joyce, M. and Chaboyer, B. (2018). Classically and Asteroseismically Constrained 1D Stellar Evolution Models of α Centauri A and B Using Empirical Mixing Length Calibrations. *ApJ* 864, 99. doi:10.3847/1538-4357/aad464

Kervella, P., Bigot, L., et al. (2017). The radii and limb darkenings of α Centauri A and B . Interferometric measurements with VLTI/PIONIER. *A&A* 597, A137. doi:10.1051/0004-6361/201629505

Kervella, P., Mignard, F., et al. (2016). Close stellar conjunctions of α Centauri A and B until 2050 . An m_K = 7.8 star may enter the Einstein ring of α Cen A in 2028. *A&A* 594, A107. doi:10.1051/0004-6361/201629201

Kim, Y.-C. (1999). Standard Stellar Models; alpha Cen A and B. *Journal of Korean Astronomical Society* 32, 119–126

Kunz, R., Fey, M., et al. (2002). Astrophysical Reaction Rate of ^{12}C(α, γ)^{16}O. *ApJ* 567, 643–650. doi:10.1086/338384

Lebreton, Y. and Goupil, M. J. (2014). Asteroseismology for "à la carte" stellar age-dating and weighing. Age and mass of the CoRoT exoplanet host HD 52265. *A&A* 569, A21. doi:10.1051/0004-6361/201423797

Lund, M. N. and Reese, D. R. (2018). Tutorial: Asteroseismic Stellar Modelling with AIMS. *ASSSP* 49, 149. doi:10.1007/978-3-319-59315-9_8

Mathur, S., Metcalfe, T. S., Woitaszek, M., Bruntt, H., Verner, G. A., Christensen-Dalsgaard, J., et al. (2012). A Uniform Asteroseismic Analysis of 22 Solar-type Stars Observed by Kepler. *ApJ* 749, 152. doi:10.1088/0004-637X/749/2/152

Metcalfe, T. S., Chaplin, W. J., Appourchaux, T., García, R. A., Basu, S., Brandão, I., et al. (2012). Asteroseismology of the Solar Analogs 16 Cyg A and B from Kepler Observations. *APJL* 748, L10. doi:10.1088/2041-8205/748/1/L10

Metcalfe, T. S., Creevey, O. L., Doğan, G., Mathur, S., Xu, H., Bedding, T. R., et al. (2014). Properties of 42 Solar-type Kepler Targets from the Asteroseismic Modeling Portal. *ApJS* 214, 27. doi:10.1088/0067-0049/214/2/27

Miglio, A. and Montalbán, J. (2005). Constraining fundamental stellar parameters using seismology. Application to α Centauri AB. *A&A* 441, 615–629. doi:10.1051/0004-6361:20052988

Nsamba, B., Monteiro, M. J. P. F. G., Campante, T. L., Cunha, M. S., and Sousa, S. G. (2018a). α Centauri A as a potential stellar model calibrator: establishing the nature of its core. *MNRAS* 479, L55–L59. doi:10.1093/mnrasl/sly092

Nsamba, B. et al. (2018b). Asteroseismic modelling of solar-type stars: internal systematics from input physics and surface correction methods. *MNRAS* arXiv:1804.04935. doi:10.1093/mnras/sty948

Paxton, B., Bildsten, L., Dotter, A., Herwig, F., Lesaffre, P., and Timmes, F. (2011). Modules for Experiments in Stellar Astrophysics (MESA). *ApJS* 192, 3. doi:10.1088/0067-0049/192/1/3

Paxton, B., Cantiello, M., Arras, P., Bildsten, L., Brown, E. F., Dotter, A., et al. (2013). Modules for Experiments in Stellar Astrophysics (MESA): Planets, Oscillations, Rotation, and Massive Stars. *ApJS* 208, 4

Paxton, B., Marchant, P., Schwab, J., Bauer, E. B., Bildsten, L., Cantiello, M., et al. (2015). Modules for Experiments in Stellar Astrophysics (MESA): Binaries, Pulsations, and Explosions. *ApJS* 220, 15. doi:10.1088/0067-0049/220/1/15

Paxton, B., Schwab, J., Bauer, E. B., Bildsten, L., Blinnikov, S., Duffell, P., et al. (2018). Modules for Experiments in Stellar Astrophysics (MESA): Convective Boundaries, Element Diffusion, and Massive Star Explosions. *ApJS* 234, 34. doi:10.3847/1538-4365/aaa5a8

Pinheiro, F. J. G. and Fernandes, J. (2013). On the (non-)universality of the mixing length parameter. *MNRAS* 433, 2893–2899. doi:10.1093/mnras/stt910

Pourbaix, D. and Boffin, H. M. J. (2016). Parallax and masses of α Centauri revisited. *A&A* 586, A90. doi:10.1051/0004-6361/201527859

Pourbaix, D., Nidever, D., et al. (2002). Constraining the difference in convective blueshift between the components of alpha Centauri with precise radial velocities. *A&A* 386, 280–285. doi:10.1051/0004-6361:20020287

Rauer, H., Catala, C., Aerts, C., Appourchaux, T., Benz, W., Brandeker, A., et al. (2014). The PLATO 2.0 mission. *Experimental Astronomy* 38, 249–330. doi:10.1007/s10686-014-9383-4

Rendle, B. M., Buldgen, G., Miglio, A., Reese, D., Noels, A., Davies, G. R., et al. (2019). AIMS - a new tool for stellar parameter determinations using asteroseismic constraints. *MNRAS* 484, 771–786. doi:10.1093/mnras/stz031

Ricker, G. R., Winn, J. N., Vanderspek, R., Latham, D. W., Bakos, G. Á., Bean, J. L., et al. (2015). Transiting Exoplanet Survey Satellite (TESS). *Journal of Astronomical Telescopes, Instruments, and Systems* 1, 014003. doi:10.1117/1.JATIS.1.1.014003

Serenelli, A. M. and Basu, S. (2010). Determining the Initial Helium Abundance of the Sun. *ApJ* 719, 865–872. doi:10.1088/0004-637X/719/1/865

Silva Aguirre, V., Davies, G. R., Basu, S., Christensen-Dalsgaard, J., Creevey, O., Metcalfe, T. S., et al. (2015). Ages and fundamental properties of Kepler exoplanet host stars from asteroseismology. *MNRAS* 452, 2127–2148. doi:10.1093/mnras/stv1388

Silva Aguirre, V., Lund, M. N., Antia, H. M., Ball, W. H., Basu, S., Christensen-Dalsgaard, J., et al. (2017). Standing on the Shoulders of Dwarfs: the Kepler Asteroseismic LEGACY Sample. II.Radii, Masses, and Ages. *ApJ* 835, 173. doi:10.3847/1538-4357/835/2/173

Söderhjelm, S. (1999). Visual binary orbits and masses POST HIPPARCOS. *A&A* 341, 121–140

Thoul, A. A. et al. (1994). Element diffusion in the solar interior. *ApJ* 421, 828–842. doi:10.1086/173695

Townsend, R. H. D. and Teitler, S. A. (2013). GYRE: an open-source stellar oscillation code based on a new Magnus Multiple Shooting scheme. *MNRAS* 435, 3406–3418. doi:10.1093/mnras/stt1533

Yıldız, M. (2007). Models of α Centauri A and B with and without seismic constraints: time dependence of the mixing-length parameter. *MNRAS* 374, 1264–1270. doi:10.1111/j.1365-2966.2006.11218.x